DOI 10.5162/sensoren2024/D4.3

Determination of the dynamic iron content in magnetorheological fluids using an indirect measurement method based on an equivalent circuit model

Thomas Wiener[1], Christina Offenzeller[1], Bernhard Jakoby[2]
[1]STIWA Advanced Products GmbH, Technologiepark 10, 4851 Gampern, Austria
[2]Johannes Kepler University, Institute for Microelectronics and Microsensors, Altenberger Straße 69, 4040 Linz, Austria

Abstract

Magnetorheological (MR) fluids are a class of smart materials with versatile applications in various engineering domains. A MR fluid consists essentially of a carrier medium (e.g. synthetic oil) with embedded magnetizable particles (e.g., carbonyl iron particles in our case). The concentration of iron in the carrier medium determines the rheological properties of the MR fluid.
The influence of the iron content in the MR fluid on the inductance of the system should be analyzed. The measurement technique investigated in our research relies on the analysis of current responses following a voltage step change which is applied to a coil magnetizing the MR under test in a test setup involving a magnetic circuit and a chamber containing the sample MR fluid. The evaluation process is conducted by means of utilizing a physically inspired model featuring lumped elements in an equivalent electrical circuit. This model is based on the T-equivalent circuit of a transformer incorporating representations of field induced eddy currents and particle motion within the MR fluid on the secondary side of the (fictitious) transformer. The model is then used to determine the inductance and to represent the electrical behavior of the actuator in a step response.

Keywords: magnetorheological fluid (MRF), T-equivalent circuit, physically inspired model, indirect measurement method, inductance measurement

1 Introduction

Magnetorheological (MR) fluids consist of small ferromagnetic particles in a carrier fluid, typically hydrocarbon oil with additives [1-4]. These particles, most commonly carbonyl iron, range in size from 1 to 10 µm. Without the presence of a magnetic field, MR fluid has a low viscosity. When exposed to a magnetic field, the particles tend to align in chain-like structures along field lines, increasing viscosity and shear stress [2,3,5,6]. This alignment occurs in two stages: first single chains are formed which then aggregate into longer and thicker structures [6,7].

Investigations are aimed at improving particle-based simulations [8], adapting MR formulations for settling and abrasion problems [3,4,9-11], optimizing designs for fast force response [12,13] and characterizing shear stress response in rotative setups [1,12,14,15]. Experimental work seeks reliable macroscopic and microscopic MR fluid models [2,16,17] and investigates the effects of particle size, distribution, and volume fraction [3,18,19]. Despite these efforts, the application of MR technology still remains limited in commercial products.

While MR fluids are currently used in devices [20,21], comprehensive models for device design are still scarcely available due to their complex response to magnetic and mechanical forces. Several studies have focused on the microstructure that influences the rheological properties of MR fluids, which are affected by magnetic fields that can lead to phenomena such as clustering and local alignment of ferromagnetic particles. This kind of complex behavior arises from the response of ferromagnetic materials to external fields, including non-linear responses, hysteresis and memory effects (remanence) [22-24].

In previous work [24] we found that in initial measurements of an actuator filled with “fresh” MR fluid, smaller shear stresses (for achieving a particular shear rate) are required compared to subsequent measurements. Even after demagnetization, this effect persisted and is thus independent of magnetically remanent behavior [24]. This means that once the MR fluid is "activated", e.g., by a first measurement

cycle, it cannot fully return to its initial state even if a demagnetization protocol is followed after each measurement. Such protocols are still useful as effects associated with remanent magnetizations and associated micro-mechanical cluster formation are also present and thus have to be eliminated to achieve reproducible measurements [24].

In the present paper we discuss an equivalent circuit, which is able to model the electric response of an actuation coil magnetizing a sheared MR fluid in a test setup introduced below. To this end, the response associated with MR fluids featuring different iron concentrations are modeled using a physics-inspired model with concentrated components, where the iron content of the fluid particularly affects the main inductance in the model. The model also considers the effects of eddy currents and mechanical time constants of the MR fluid. Finally, the model relates the modelled inductance to the dynamic iron content in the fluid, which may then be used to predict shear stresses.

2 Material and methods

2.1 Material

The MR fluids used in these studies are two different commercial fluids supplied by LORD Corporation (USA). The first (type MRF-122EG) consists of synthetic oil (hydrocarbon based) and a volume concentration $\Phi = 22$ vol% of carbonyl iron particles featuring a diameter in the range of 1 to 10 µm. The second MR fluid MRF-140BC is the same as in [24] and consists of $\Phi = 40$ vol% iron particles.

To ensure accurate measurement conditions and to avoid non-uniform particle distribution due to sedimentation, the MR fluids had to be thoroughly redispersed. First, the MR fluid container was placed on a uniaxial mixer for at least two hours to homogenize and dissolve any residual iron. A biaxial shaker was then used to break up potential particle agglomerates by rotating the container for at least 20 minutes (for more details see [24]).

From the analyses in [24], we know that the mixing routine redispersed the MR fluids well and that the particles are sufficiently dissolved in the fluids. We therefore suppose that the stated iron concentrations are initially in agreement with the ones stated in the manufacturer's data sheet (22 and 40 vol%).

2.2 Experimental setup

The custom experimental setup (Fig. 1) resembles a parallel plate magneto-rheometer used for shear mode [16,23,25] characterization of MR fluid. It comprises three key components: a stator (green), a MR fluid chamber (light red), and a rotor (yellow). The stator contains the MR fluid and houses a rotating disc, part of the rotor which is driven by a servo motor.

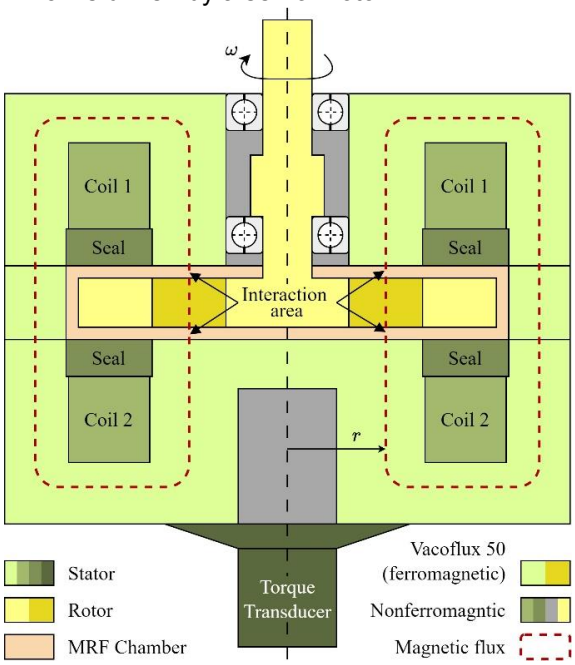

Fig 1: Schematic of the experimental setup for the measurement of the MR fluid in shear mode (cross section). The coil wires intersect this cross section orthogonal to the drawn plane.

Magnetic flux ("flowing" along the red dashed lines in Fig. 1) is generated by two coils (Coil 1 and 2) within the stator, oriented in the same direction. The coils are powered by a custom power supply controller and can produce a magnetic flux density of 2.3 T. The stator and rotor are made of *Vacoflux 50*, a material with high magnetic permeability featuring a high saturation magnetization (which is, however, never reached in our experiments). Other components, like the sealing system, are nonferromagnetic.

Inside the MR fluid chamber, there are two interaction areas (or working gaps) where the adjustable magnetic field interacts with the MR fluid, generating shear forces. The coils' geometry ensures a uniform field distribution across these gaps, which are located at the top and bottom of the disc.

A more detailed description of the structure and the calculated magnetic field strengths in

the interaction areas from finite element calculations can be found in [24].

Sedimentation is not an issue for the setup because, first, the design of the chambers is flat, so gravity has little effect on particle distribution. Second, our measurements were taken within a maximum of two hours after filling with homogenized MR fluid, therefore in this short time there will be no sedimentation of particles in the liquid [9].

Note that the setup was not particularly designed to keep eddy currents low, since the focus was on achieving high field strengths and a constant field distribution in the interaction area. The eddy currents that do occur cannot be neglected and must be accounted for in the model.

2.3 Inductance measurement of the magnetization coil

Inductance can be measured in several ways. A very common method is to apply a voltage step to the inductance to be measured and analyze the step response of the current, which should correspond to a first-order lag element (*PT1*) for an ohmic-inductive load. Evaluating the time τ it takes the current to reach 63 % of the final stationary value, one can calculate the inductance L from the relationship $\tau = L/R$, given that the resistance R is known.

However, the experimental setup does not behave like a simple first-order lag element (*PT1,* see Fig. 2) due to non-ideal properties such as eddy currents and motion of iron particles in the MR fluid (see section “Results”). Measuring inductance using a *LCR* meter or phase shift between current and voltage with sinusoidal excitation is therefore not feasible. There is little information in the literature on the measurement of inductance in MR actuators or on variable inductance during operation.

Therefore, we pursued an indirect route through the complete analysis and curve fitting via a physically inspired model and calculations in *LTspice* that capture eddy currents, motion, and the main inductance.

The electrical quantities were recorded using a digital storage oscilloscope (Tektronix mixed signal oscilloscope *MSO54B* (350 MHz, 6.25 GS/s)) with a probe and a current clamp. Power was supplied by a laboratory power supply (Korad *KA3005P*, with an internal resistance modeled in *LTspice* with $R_i = 0.1\ \Omega$, see Fig. 3). The applied voltage jump (from 0 to 9 V) was implemented using a customized circuit board with H-bridges, realized with field effect transistors with a resistance of $R_{FET} = 0.3\ \Omega$ each, to produce a steep jump within milliseconds.

3 Results

The aim of the investigations is to be able to make an indirect statement about the iron content in the interaction area via the inductance behavior of the actuator and subsequent predictions of generated shear stress response. The hypothesis of [24] is that chain formation and other effects lead to an accumulation of iron particles in the interaction area and an increasing iron concentration, which contributes to an initial irreversible MR fluid activation.

In order to obtain a first basic electrical model for the coil in Fig. 1, the first measurement is carried out with an empty chamber, i.e. with air as a test medium.

Figure 2 shows the voltage response at the coil terminal in blue (*Voltage*) and the current curve in red (*i(0 vol%)*) for air-filling. The solid lines are the data recorded by the oscilloscope. The voltage jumps to a value of $u_0 = 9$ V at time instant $t = 0$ s, collapses a little due to the ohmic losses of the internal resistance of the power supply and the H-bridge, and stabilizes at a value of $u_S = 8.53$ V in the steady state area. At first sight the current response may appear to show *PT1* behavior (as it would be for an *RL* series circuit or a lossy coil). However, closer inspection reveals that a second time constant due to eddy currents is involved.

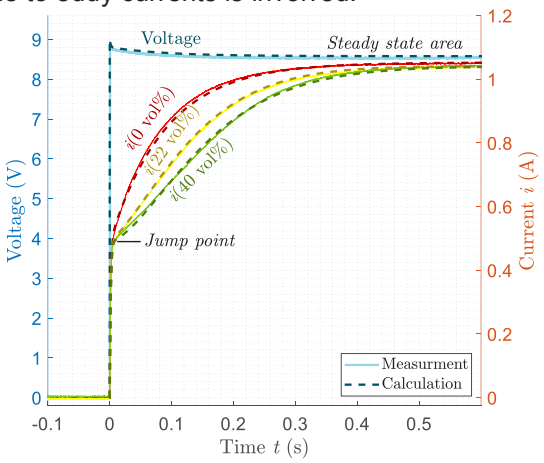

Fig. 2: Current and voltage curves of the measurement and calculation with LTspice of the step response, applied to the experimental setup: 0 (red), 22 (yellow) and 40 vol% (green) iron content in the MRF chamber.

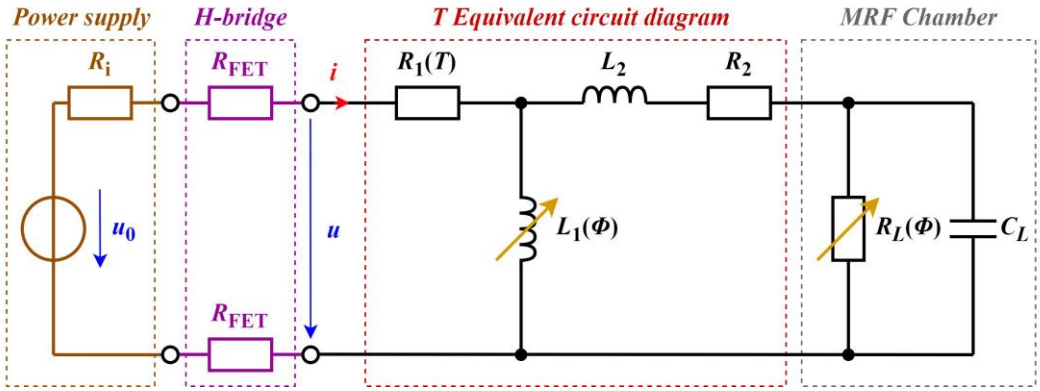

Fig. 3: Phenomenological electrical equivalent circuit diagram of the experimental setup.

To analyze this behavior, a model was built in *LTspice* and fitted to the measured data. The starting point for the physics-inspired electrical diagram is the T-equivalent diagram of a transformer. Figure 3 shows the electrical diagram used for the simulation, with the source and H-bridges shown on the left.

In the equivalent circuit, following values are used: the main inductance $L_1(\Phi)$, the stray inductance L_2, a resistor R_2 representing the eddy currents, a load, which was phenomenologically modelled as a R_L-C_L parallel circuit representing the MRF-chamber, the temperature dependent ohmic coil resistance $R_1(T)$, the ohmic half bridge resistors R_{FET} and ohmic internal resistor of the source R_i.

The ohmic components R_i, R_{FET}, $R_1(T)$ were measured with a resistance meter.

After the voltage jump, the current stabilizes at $t > 0.3$ s, to a steady state value of about $I_S = 1.05$ A (see Fig. 2), which is essentially related to the ohmic resistance R_1 in the model. R_1 is the ohmic resistance of the supply line and the coils (which is temperature dependent and has a value of 7.8-8.2 Ω) and in particular determines the level of the steady-state current value I_S.

R_2 represents losses due to eddy currents in the magnetic core of the circuit and L_2 represents the stray inductance involved in this coupling (just as in the classical transformer model). The main core material of the experimental setup is *Vacoflux 50*, which has good properties for high saturation field strengths and is designed as a solid material. This results in significant eddy currents which strongly influence the current curve in case of transients. The initial point the current almost instantly jumps to (see Fig. 2) is essentially determined by R_2 and L_2 yielding a much smaller time constant compared to the one associated with the main inductance. The values for L_2 and R_2 can be readily determined from the height and the delay of the initial jump, which is virtually the same for all measured cases (see “Jump point” in Fig. 2). This is consistent with the eddy current interpretation as the eddy currents in the magnetic core, which is present for both measurements in air and with MR fluids.

Furthermore, R_i, R_{FET}, $R_1(T)$, R_2 and L_2 are the same for all measurements and have been assumed to be constant.

The remaining three fit parameters (L_1, R_L and C_L) in the equivalent circuit were identified by curve fitting and minimizing the error.

L_1 is the main inductance that significantly determines the current curve and has been determined to have a value of $L_1(0\ \text{vol\%}) = 420$ mH for air filling of the gap. The “secondary load” $R_L \parallel C_L$ corresponds to a short circuit $R_L(0\ \text{vol\%}) = 0\ \Omega$ for air filling. Figure 2 shows the calculated results for current and voltage plotted against the measured data. The model agrees well with the measured data despite the simple model structure. To test the model’s robustness we verified that, without fitting anew, it also reasonably holds for measurements featuring a 12 V jump and in case of impressing a stationary current injection by using an artificial source series resistor of 100 Ω (not shown here).

Next, the chamber of the experimental setup was filled with fresh (unused) MRF-140BC with an initial concentration of $\Phi = 40$ vol% iron homogeneously distributed in the liquid. Our expectation for the equivalent circuit diagram is that the main inductance L_1 should increase.

In Fig. 2 the green curve shows the current measurement for 40 vol% iron. The current

takes longer to reach the steady state value of I_S. The jump point is approximately the same as at $\Phi = 0$ vol%. A third time constant can be seen.

The following values are identical at 40 vol% as with the first measurement with air filling and support the quality of the model: R_i, R_{FET}, $R_1(T)$, R_2 and L_2.

Only three parameters were varied to fit the measured responses for MR fluid filling: the main inductance L_1 and the load (R_L, C_L).

Instead of a short circuit, R_L(40 vol%) had now a value of 12 Ω and C_L = 0.01 F is found. This load is supposed to model movement of the iron particles when aligning with the field, which introduce a mechanical time constant related to C_L. R_L also contributes to this time constant and represents eddy current (and other losses) in the MR fluid.

The main inductance L_1 increases as expected with increasing iron concentration in the fluid to L_1(40 vol%) = 750 mH, an increase of 79%. The results of the calculation with *LTspice* are shown in Fig. 2 as dashed lines. Despite the concentrated elements in the rather simple model, there are hardly any deviations between measurement and calculation.

To verify the electrical equivalent circuit diagram, a further measurement was carried out with an MR fluid containing $\Phi = 22$ vol% iron concentration, which is approximately halfway between 0 and 40 vol%. The measured and calculated results are shown in Fig. 2 in yellow, with dashed line representing the calculation from the *LTspice* model. The obtained fitting parameters are L_1(22 vol%) = 610 mH and R_L(22 vol%) = 10 Ω. All other component values are identically as for 0 and 40 vol%.

As expected, the curve for 22 vol% iron concentration lies between the curves for 0 and 40 vol%. The results calculated with the fitted parameters (L_1 and R_L) are in good agreement with the measurement.

4 Conclusion

A main contribution of this work is the development of a new method to indirectly determine the variation of the iron content in MR fluids by analyzing the equivalent circuit of the experimental setup, where the MR fluid under consideration is contained in a sample chamber embedded within a magnetic circuit. This approach is supported by a physically inspired model that accounts for non-ideal properties such as eddy currents in the magnetic circuit and the MR fluid as well as mechanical relaxation effects of the particles in the MR fluid.

5 Appendix: Model values

Tab. 1: Constant values of the physically inspired model.

	Values	Physical description
u_0	0-9 V	Power supply
R_i	0.1 Ω	Resistance of the source
R_{FET}	0.3 Ω	Resistance of the H-bridge
$R_1(T)$	7.8 – 8.2 Ω	Resistance of the windings (temperature dependent)
L_2	30 mH	Stray inductance (eddy currents)
R_2	10.5 Ω	Resistance due to eddy currents
C_L	10 mF	MRF-Chamber (movement)

Tab. 2: Concentration-dependent values of the physically inspired model.

Φ	0	22	40	vol%
$L_1(\Phi)$	0.42 H	0.61 H	0.75 H	Main inductance
$R_L(\Phi)$	0 Ω	10 Ω	12 Ω	MRF-Chamber (movement)

References

[1] Rabinow, J. (1948). The Magnetic Fluid Clutch. *Transactions of the American Institute of Electrical Engineers*, **67(2), 1308–1315**. https://doi.org/10.1109/t-aiee.1948.5059821

[2] Tao, R. (2001b). Super-strong magnetorheological fluids. *Journal of Physics: Condensed Matter*, **13(50), R979–R999**. https://doi.org/10.1088/0953-8984/13/50/202

[3] Jolly, M., Bender, J. W. & Carlson, J. D. (1999). Properties and Applications of Commercial Magnetorheological Fluids. *Journal of Intelligent Material Systems and Structures*, **10(1),** 5–13. https://doi.org/10.1177/1045389x9901000102

[4] Carlson, J. D. (2002). What Makes a Good MR Fluid? *Journal of Intelligent Material Systems and Structures*, **13(7–8), 431–435.** https://doi.org/10.1106/104538902028221

[5] Wang, Y., Luo, Q., Liu, H., Wu, J., Lian, M. & Li, T. (2019). Aggregated chain morphological variation analysis of magnetorheological fluid (MRF) in squeeze mode. *Smart Materials and Structures*, **28(10), 105038.** https://doi.org/10.1088/1361-665x/ab39f9

[6] Jolly, M. R., Bender, J. W., & Mathers, R. T. (1999). Indirect measurements of microstructure development in magnetorheological fluids. *International Journal of Modern Physics B* (**Vol. 13**). https://doi.org/10.1142/S0217979299002113

[7] Kubík, M., Válek, J., Žáček, J., Jeniš, F., Borin, D., Strecker, Z., & Mazůrek, I. (2022). Transient response of magnetorheological fluid on rapid

change of magnetic field in shear mode. *Scientific Reports*, **12(1).** https://doi.org/10.1038/s41598-022-14718-5

[8] Sherman, S. G., Paley, D. A., & Wereley, N. M. (2011). Massively Parallel Simulations of Chain Formation and Restructuring Dynamics in a Magnetorheological Fluid. *ASME 2011 Conference on Smart Materials, Adaptive Structures and Intelligent Systems, Volume 1* https://doi.org/10.1115/SMASIS2011-5188

[9] Choi, Y., Xie, L. & Wereley, N. M. (2016). Testing and analysis of magnetorheological fluid sedimentation in a column using a vertical axis inductance monitoring system. Smart Materials and Structures, 25(4), 04LT01. https://doi.org/10.1088/0964-1726/25/4/04lt01

[10] Chambers, J. M. & Wereley, N. M. (2017). Vertical axis inductance monitoring system to measure stratification in a column of magnetorheological fluid. IEEE Transactions on Magnetics, 53(1), 1–5. https://doi.org/10.1109/tmag.2016.2606345

[11] Portillo, M. A., & Iglesias, G. R. (2017). Magnetic nanoparticles as a redispersing additive in magnetorheological fluid. Journal of Nanomaterials, 2017, 1–8. https://doi.org/10.1155/2017/9026219

[12] Güth, D., Schamoni, M. & Maas, J. (2013). Magnetic fluid control for viscous loss reduction of high-speed MRF brakes and clutches with well-defined fail-safe behavior. *Smart Materials and Structures*, **22(9), 094010**. https://doi.org/10.1088/0964-1726/22/9/094010

[13] Horváth, B., Decsi, P., & Szalai, I. (2022). Measurement of the response time of magnetorheological fluids and ferrofluids based on the magnetic susceptibility response. *Journal of Intelligent Material Systems and Structures*, **33(7),** 918–927. https://doi.org/10.1177/1045389X211038697

[14] Jackel, M., Kloepfer, J., Matthias, M. & Seipel, B. (2013). The novel MRF-ball-clutch design – a MRF-safety-clutch for high torque applications. *Journal of physics*, **412, 012051**. https://doi.org/10.1088/1742-6596/412/1/012051

[15] Böse, H., Gerlach, T. & Ehrlich, J. (2013). Magnetorheological torque transmission devices with permanent magnets. *Journal of physics*, **412, 012050**. https://doi.org/10.1088/1742-6596/412/1/012050 https://doi.org/10.1016/j.partic.2013.03.002

[16] Lagger, H. G., Bierwisch, C., & Moseler, M. (2013). MRF in a plate-plate magnetorheometer: Numerical insight into the particle-wall interface. Journal of Physics, 412, 012020. https://doi.org/10.1088/1742-6596/412/1/012020

[17] Dorfmann, L., Ogden, R. W., & Wineman, A. S. (2007). A three-dimensional non-linear constitutive law for magnetorheological fluids, with applications. International Journal of Non-Linear Mechanics, 42(2), 381–390. https://doi.org/10.1016/j.ijnonlinmec.2007.03.002

[18] Sarkar, C. & Hirani, H. (2015). Effect of Particle Size on Shear Stress of Magnetorheological Fluids. *Smart Science*, **3(2), 65–73.** https://doi.org/10.1080/23080477.2015.11665638

[19] Gudmundsson, K., Jonsdottir, F., Thorsteinsson, F. & Gutfleisch, O. (2011). An Experimental Investigation of Unimodal and Bimodal Magnetorheological Fluids with an Application in Prosthetic Devices. *Journal of Intelligent Material Systems and Structures*, **22(6), 539–549**. https://doi.org/10.1177/1045389x11403821

[20] "DISCOVER HAPTICORE." XeelTech. https://www.xeeltech.com/hapticore/ (accessed Mar 25, 2024)

[21] "Hapticore." STIWA. https://www.stiwa.com/en/manufacturing/advanced-products/hapticore (accessed Mar 25, 2024)

[22] Rankin, P. J., Horvath, A. T., & Klingenberg, D. J. (1999). Magnetorheology in viscoplastic media. *Rheologica Acta*, **38(5), 471–477**. https://doi.org/10.1007/s003970050198

[23] Shan, L., Chen, K., Zhou, M., Zhang, X., Meng, Y., & Tian, Y. (2015). Shear history effect of magnetorheological fluids. *Smart Materials and Structures*, **24(10).** https://doi.org/10.1088/0964-1726/24/10/105030

[24] Wiener, T., Offenzeller, C., Martetschläger, D., Wimmer, D., Spirowski, T., & Jakoby, B. (2024b). Phenomenological studies on magnetic and mechanical remanence effects in magnetorheological fluids. Smart Materials and Structures. https://doi.org/10.1088/1361-665x/ad2aa7

[25] Zheng, J. N., Li, Y. Z., Chen, C., & Chen, S. M. (2020). The sealing properties of magnetorheological fluids under quasi-static tensile. *Smart Materials and Structures*, **29(10).** https://doi.org/10.1088/1361-665X/aba53f